ELSEVIER

Ceramics International 25 (1999) 731–738

CERAMICS INTERNATIONAL

# Early-stage sintering in a powder compact of polyhedral particles II. Experimental analysis with a highly sinterable $Al_2O_3$

Takayasu Ikegami*, Yoshizou Kitami, Masayuki Tsutsumi

*National Institute for Research in Inorganic Materials, 1-1, Namiki, Tsukuba-shi, Ibaraki 305, Japan*

Received 3 March 1998; accepted 19 May 1998

**Abstract**

A model of early-stage sintering for polyhedral particles is examined with a highly sinterable $Al_2O_3$ powder. Combining of the initial and intermediate stages based on the model concerned describes quantitatively its sintering data such as power dependence of time and reduction in a specific surface area. Valid estimations of a model and/or mechanisms of sintering necessitate the accurate measurement of both shrinkage versus sintering time and specific surface area versus shrinkage. 

*Keywords:* A. Sintering; B. Microstructure-prefiring; C. Diffusion; D. $Al_2O_3$; Polyhedral

## 1. Introduction

Conventional powder processing [1,2] has generally produced ceramics powders with hard agglomerates, which have well grown necks, a kind of face contacts between particles. Usual sintering models [3–5] for the initial stage, on the other hand, assume essentially a point or a line contact for necks before sintering begins. The difference in geometry between a real neck and a model neck has caused serious controversies [6,7] for the kinetic studies of the initial stage. Severe criticisms also resulted from various phenomena such as (1) appreciable reduction [8,9] in the surface area of a powder compact at a relatively low temperature, (2) a different densification rate [10] from a micro-region to another micro-region in a powder compact, (3) degassing [11] of adsorbed molecules from the surfaces of particles at a sintering temperature, etc.

Recent development of powder processing technologies, however, has brought about well-sinterable powders for both oxide [12,13] and non-oxide [14] ceramics. Such powders usually consist of very soft agglomerates or quasi-monodispersed particles, and so the green compact of them has negligibly grown necks. The necks concerned, thus, consist of the model neck of the initial stage at the geometrical point of view, avoiding one of the aforesaid controversies. Furthermore, a sinterable $Al_2O_3$ powder [15] is, in particular, favorable to the kinetic study of sintering for the following reasons; (i) well sinterability of a highly pure $Al_2O_3$ powder with no additive; (ii) the low reactivity against various gasses; (iii) the large particle size of a usual raw $Al_2O_3$ powder (several 100 nm), which is nearly 10 times as large as those (several 10 nm) of other refractory oxides powders such as MgO, $Y_2O_3$, $Y_2O_3$-doped $ZrO_2$, etc. The property of (i) suggests a slight influence of impurities on the sintering of such an $Al_2O_3$ powder. The characters of (ii) and (iii), on the other hand, indicate not only a small amount of adsorbed gasses on the raw $Al_2O_3$ powder but also a large density of its green compact. The present powder, for example, reduced its weight only by 0.1 wt% even after firing at 1100°C. Its green density, also, was larger than 59% of theoretical, which is near to the random closest density [16], 63%, for ball bearings, equal sized spheres. Such a large density suggested a few micro-regions in which particles are packed loosely, and new particle-to-particle contacts rarely occurred during sintering. Furthermore, recent surface area measurement [17] showed negligible neck growth for the present sample before practical densification occurred. Since, thereby, the present sample ruled out most of the origins for the aforesaid controversies, its sintering behaviors were examined with a sintering model for polyhedral particles (Part I) [18].

* Corresponding author.

0272-8842/99/$ - see front matter 
PII: S0272-8842(99)00075-9

## 2. Experimental procedures

A purchased $Al_2O_3$ powder (AKP-20, Sumitomo Chem. Co. Ltd., Osaka, Japan and major impurities of Si = 15, Na = 3, Ma = 3, Cu < 1 and Fe = 8 in ppm by weight) was already ball-milled in the half-way of the fabrication process in its supplier to collapse agglomerates of primary particles. The powder concerned was suspended in ethyl alcohol, heated to dryness at 70°C and calcined at 800°C for 2 h in flowing $O_2$. The resulting powder was formed into disks under a pressure of 30 MPa and then hydrostatically pressed at 200 MPa.

The shape of particles in the powder was observed by transmission electron microscopy (TEM)(JEM-2000EX, JEOL Co., Tokyo, Japan). Shrinkage of the powder compacts, ΔL, was measured with a thermo-mechanical analyzer, TMA (TMA-1700, Rigaku Co., Tokyo, Japan) during constant-rate heating (CRH). A heating rate of 30°C/min to approximately 50°C/min was chosen for isothermal heating (IH), up to a given temperature, at which the disk was held for a given time, and then quenched down to room temperature. The density of the green compact, $\rho_s$, and those of isothermally sintered compacts, $\rho_d$, were calculated from dimensions and weights. The fractured surfaces were observed by scanning electron microscopy (SEM) (S-5000, HITACHI Co., Tokyo, Japan), and an average radius, $R_{se}$, was calculated on the basis of about 250 grains. The specific surface areas of both the powder compact, $S_{ps}$, and sintered compacts, $S_p$, were determined by the BET method with nitrogen at −196°C using an automatic surface area analyzer (Model 4201, Beta Scientific Co., Long Island, U.S.A.).

A pressure for compaction increased contact areas between particles in the green compact, creating a measurable relation between $S_{ps}$ and applied pressure. The areas of grown necks in hard agglomerates, however, seemed to be unchanged irrespective of an applied pressure. Such grown necks do not contribute to decrease of the $S_{ps}$ value by pressing, disturbing valid estimation of the aforesaid relation. Water sedimentation was, then, applied to the purchased powder to eliminate such agglomerates.

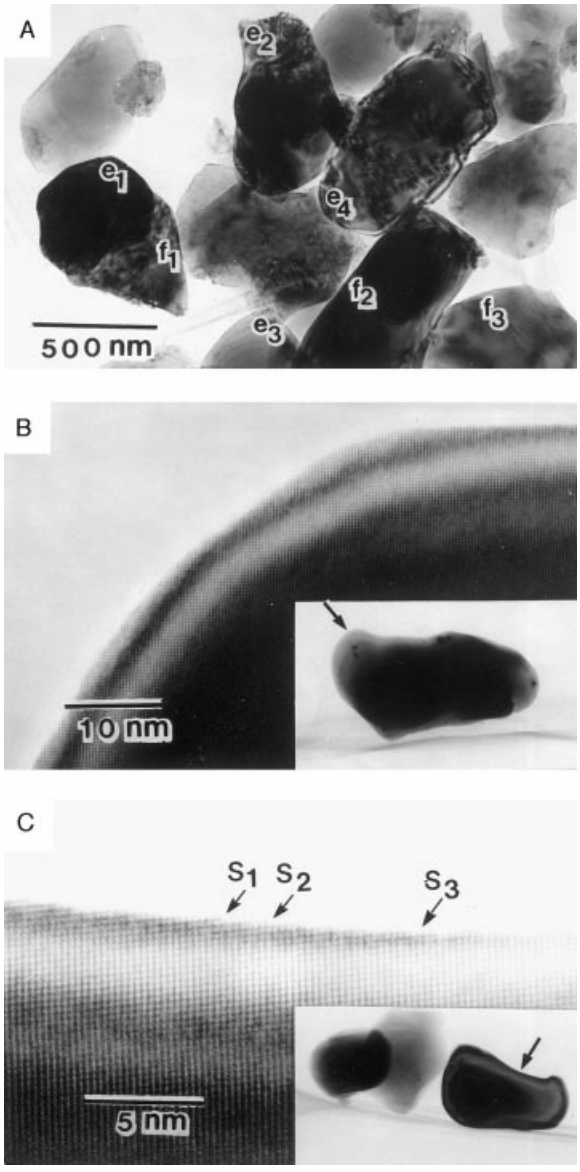


Fig. 1. TEM micrographs of $Al_2O_3$ powder. (A) round edges ($e_1$, $e_2$, - -) and slightly curve or flat surfaces ($f_1$, $f_2$, - -), (B) a smoothly curved edge with no clear facet and (C) steps ($s_1$, $s_2$, - -) on a slightly curved face.

## 3. Results

Fig. 1A shows that the majority of the starting particles have both round edges ($e_1$,$e_2$, - -) and slightly curved or flat surfaces ($f_1$, $f_2$, - -). An enlarged TEM microphotograph of Fig. 1B shows no clear facet on a smoothly curved edge. Fig. 1C, on the other hand, shows steps ($s_1$, $s_2$, - -) on a slightly curved surface. The $\rho_s$, $R_{se}$, and $S_{ps}$, values of the green compact pressed at 200 MPa were 59.2% of theoretical, 160 nm and 4.7 m/g, respectively. Fig. 2 shows typical fractographs of (A) the green compact of the calcined powder, (B) the compact sintered at 1225°C for 960 min, and (C) the green compact of the sedimented powder. Fig. 3 shows the CRH shrinkage curves of the present sample, which give 1/3.8–1/5.2 for the time exponent, $1/n$, of kinetic equations of sintering. The activation energy for densification fell from 1020kJ/mol at about ΔL = 0.3% to 500 kJ/mol above ΔL = 2%. Fig. 4 shows the isothermal shrinkage curves, with slopes of 1/4 to approximately 1/6, which equal the $1/n$ values. Densification of the sedimented powder occurred at a temperature region lower than that of the calcined powder. There was, however, slight difference in sintering character, both the E and the $n$ values, between those powders. Fig. 5 shows negligible grain growth in the region from ΔL = 0 to = 4.1%. The

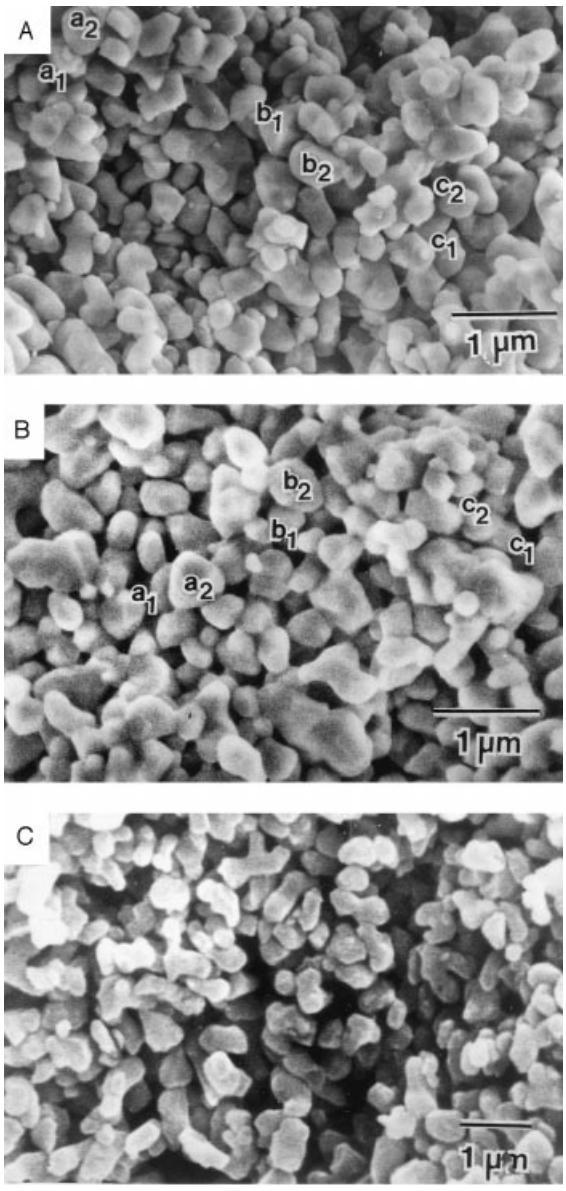


Fig. 2. Typical fractographs of (A) the green compact, (B) a compact sintered at 1225°C for 960 min, $\Delta L = 6.8\%$, and (C) the green compact of sedimented particles.

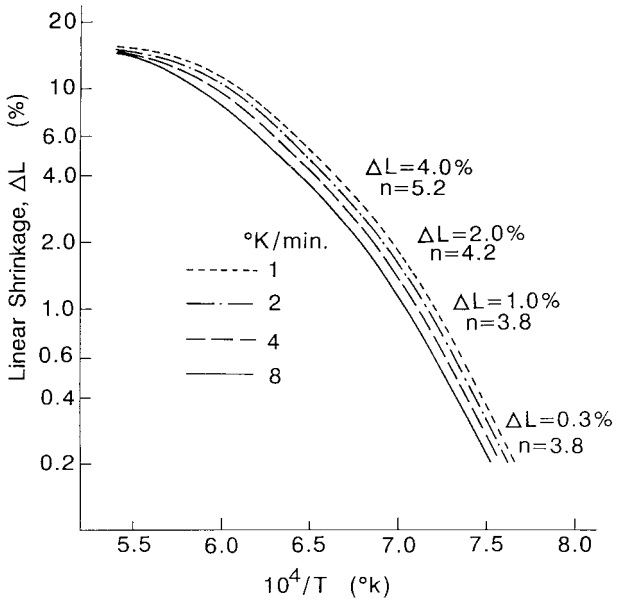


Fig. 3. Experimental CRH shrinkage of Al $_2$O $_3$ compacts as a function of a reverse temperature.

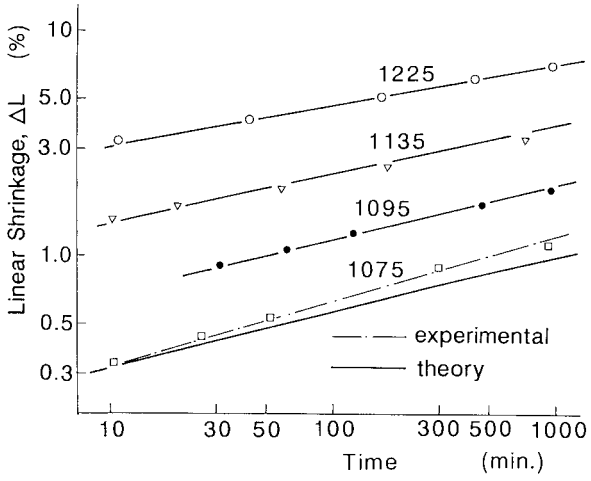


Fig. 4. Isothermal time dependence of shrinkage of $Al_2O_3$ compacts at 1075, 1095, 1135 and 1225°C. The solid lines were calculated from Eqs. (2)–(5). Dots were experimentally obtained.

$S_p$ value in Fig. 6 decreased rapidly in the early stage of sintering until ΔL of 1.5%, followed by almost a linear variation later. Fig. 7 shows that increase of a compaction pressure resulted in no negligible decrease in the $S_{ps}$ value for the sedimented powder. The data concerned, then, indicated increasing contact areas between particles in the powder compact.

## 4. Discussion

There are many kinds of alumina [19] such as amorphous, η-, γ-, χ-, α- $Al_2O_3$. The α-type is the most stable crystal structure because the others transform to α-$Al_2O_3$ at a temperature higher than about 1000°C. To avoid the non-uniform densification due to the transformation, a raw alumina powder has been usually calcined at about 1200°C, which is appreciably higher than those of other refractory oxide powders. The former powder is markedly larger in size than the latter ones in general.

Herring [20] estimated the difference, $\Delta\mu$, in the chemical potentials of atoms between beneath a curved neck and a flat surface as

$$\Delta\mu = \gamma\Omega\left(\frac{1}{r_1} - \frac{1}{r_2}\right) \quad (1)$$

where $r_1$ and $r_2$ are the principal radii of curvature of the neck, $\gamma$ is the surface free energy, and Ω is atomic

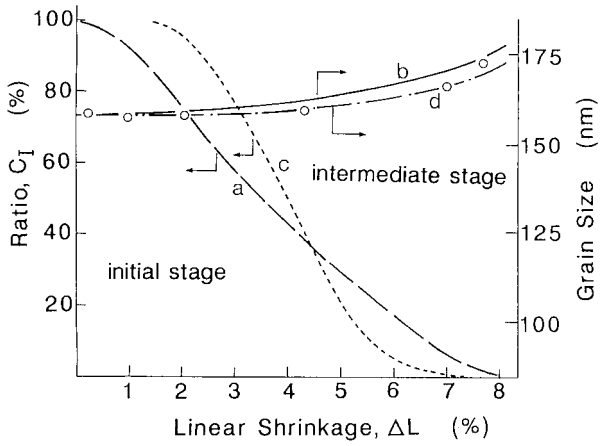


Fig. 5. Grain growth and a number ratio of necks, $C_I$, of the initial stage remaining in a sintered compact to all the starting contacts in the green compact. Lines a and b show the values of $C_I$ and grain sizes based on the present model, and lines c and d show those based on Coble's model [5], respectively. Dots were experimentally obtained.

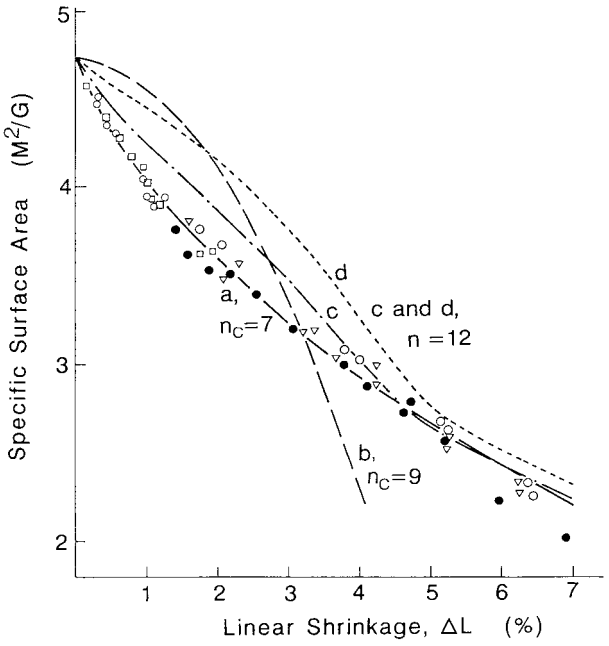


Fig. 6. A specific surface area as a function of shrinkage. Line a is obtained from Eq. (7). Lines b, c and d are calculated based on Bannister's model [25] (Fig. 1B in Part I) and the usual model (Fig. 1A [5] in Part I and the convex surface model [30]), respectively.

volume. Eq. (1) indicates that a clean-cut edge has the much higher $\Delta\mu$ than the neighboring places because of its very small radius of positive curvature of the surface. To reduce the high chemical potential, the round edges in Fig. 1 appeared instead of the clean-cut edges in the present powder. High resolution TEM [21,22], on the other hand, sometimes showed many facets on a curved surface instead of a smoothly curved surface. Facets are flat surfaces, which apparently contrast with curved surfaces in geometric character. Eq. (1) was, however, derived under the condition that increase of the surface

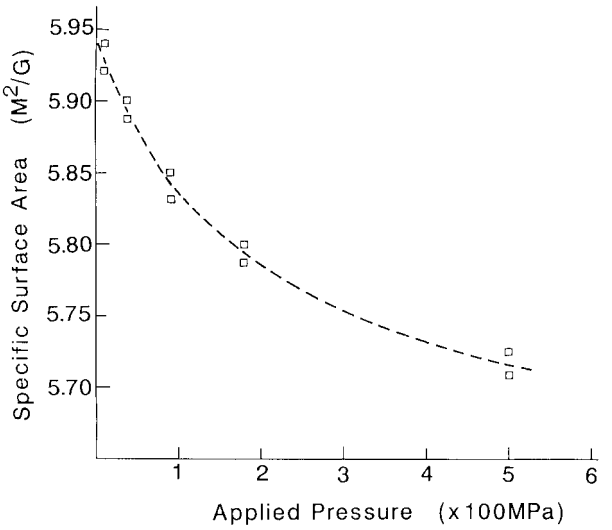


Fig. 7. Decrease of a specific surface area by an applied pressure. Dots were experimentally obtained.

free energy by increasing a small hump of volume is just compensated by decrease of the Helmholtz free energy. Its derivation required no condition for the array of atoms on the surface. If, then, a number of facets is so large that there are many facets on the aforesaid small hump, Eq. (1) can evaluate the average chemical potential of atoms on such a surface.

The present particles were so large that it was difficult to observe thoroughly, atomic arrays on the round surfaces of the edges by TEM. Steps on the slightly curved surface, however, can be observed in Fig. 1C, proving the fine resolution on the present TEM observation. Even if, then, the round edge consisted of facets, the smooth curvature of the edge concerned indicated negligibly smaller sizes of facets than those of the edge. The radii of curvature of neck surfaces were, also, estimated to be appreciably larger than those of the facets on them. These evaluations suggest that Eq. (1) can approximate to the chemical potential of atoms at the neck surfaces.

Wulff construction [23], on the other hand, suggests flat polyhedral faces for a crystalline particle. The particle shapes in Fig. 1, therefore, must be governed by both this condition and Eq. (1). The areas of the round edges are very small in comparison with those of the flat or slightly curved surfaces. The present particles were closer in shape to the polyhedral particles assumed in Part I [18] than to spherical particles.

Mobility of atoms abruptly increases with elevating a firing temperature, and, thus, the highest temperature governs both the size and the shape of particles in general. The $S_P$ value must change slightly till a firing temperature is elevated near to the calcination temperature. The present $S_P$ value [17] appreciably decreased even in a low temperature region like 700–1100°C. Such reduction has usually been explained with neck growth by the surface

diffusion mechanism [8,9]. Compaction increases a coordination number among particles, that is, a number of necks. If the usual explanation had been valid, the $S_P$ value would have decreased more quickly for a powder compact with many necks than for the loose powder with relatively fewer necks during firing. The present experimental data showed a slight difference in the $S_P$ value between the loose powder and the powder compact at a lower temperature than 950°C. Inconsistency of the experimental data with the usual explanation suggested negligible neck growth in such a temperature range. The following three successive phenomena [17] were considered; (1) ball-milling after calcining at about 1200°C produced not only particles with rough surfaces but also small flakes; (2) reduction in $S_P$ occurred initially through both smoothing of the rough surfaces and disappearance of the small flakes up to 950°C and then (3) proceeded along with noticeable densification due to neck growth from 950°C. Since the calcination temperature (≈1200°C) was markedly higher than 950°C, the concurrent phenomena, the reduction in $S_P$ and simultaneous densification, may be attributable to the thermodynamically unstable geometry, point or line contacts formed by compaction of the powder. The particles with such contacts have a large surface area considering the volume of them. The excess surface free energy due to the large surface enhanced neck growth at the contacts even at the aforesaid low temperature.

Reported models [3–5,24–27] for initial-stage sintering describe neck growth with a unique angle $\theta$ between faces of particles forming the neck. Dispersed $\theta$ values, however, must be expected for necks between polyhedral particles in a powder compact. Necks with a smaller $\theta$ value grow quickly in comparison with those with a larger $\theta$ value in general. Geometrical change of necks between the initial and the intermediate stage occurs gradually from necks with a smaller $\theta$ value to those with a larger one during densification. The initial stage and the intermediate stage, thus, combine in such a sintering system. The theoretical study of Part I [18] gave the number ratio, $C_I$, of necks of the initial stage remaining in a sintered compact to all of the starting line contacts in the green compact as

$$C_I = \frac{30 - \theta_i}{30} \tag{2}$$

where $\theta_i$ is the critical angle of $\theta$ at which the neck geometry changes from the initial to the intermediate stage. The $C_I$ value calculated from Eq. (2) is shown by the long dashed line, a, in Fig. 5.

SEM fractographs in Fig. 2 show many particles partially covered ($a_1$, $b_1$ - -) by other neighboring particles ($a_2$, $b_2$ - -). Since the measured radii of the particles were smaller than the actual values accordingly, the average radius of particles, $R$, for the powder was estimated from the relation of $R = 3/\rho_t S_{ps}$, where $\rho_t$ is the theoretical density. The present variation of $\rho_d$ was relatively narrow between 59.2 and 76, suggesting slight change in packing geometry of particles. It was assumed that the aforesaid covering of particles reduced the mean radius of particles, $R_m$, by the same degree irrespective of densification. If this is the case, the ratio of $R_s/R_g$ estimates a relative degree of grain growth during sintering with a small error, where $R_s$ and $R_g$ are, respectively, $R_{se}$ for a sintered compact and the green compact. The $R_m$ value, then, was estimated from $R_m = R_s R/R_g$.

Densification proceeds together with grain growth in the intermediate stage in general. A previous study [28] related the degree of grain growth to that of densification

$$\log\left(\frac{R_j}{R}\right) = K_G \log\left[\frac{\rho_j(1-\rho_i)}{\rho_i(1-\rho_j)}\right] \tag{3}$$

where $K_G$ is a constant (=0.259) dependent on the grain size distribution, $\rho_j$ is the relative density of a microregion, and $R_j$ is a mean radius of particles in the microregions of the density $\rho_j$ where the intermediate stage began at the density of $\rho_i$. Eq (3) indicates that when the intermediate stage starts at a lower $\rho_i$ value, that is, at an earlier stage, the larger $R_j$ value results. As mentioned before, the starting density, $\rho_i$, increases with increase of the $\theta_i$ value. The $R_m$ value [18] for a sintered compact is, then, calculated from

$$R_m = R\left(1 - \frac{6\theta_i}{\pi}\right) + \frac{6R}{\pi}\int_0^{\theta_i}\left[\frac{\rho_j(1-\rho_i)}{\rho_i(1-\rho_j)}\right]^{K_G} d\theta \tag{4}$$

The first and the second terms in the right-hand side of this equation evaluate the contribution of particles to the $R_m$ value still in the initial stage and already in the intermediate stage, respectively. Line b in Fig. 5 shows the calculated $R_m$ value, which increased by 5% of the $R$ value during densification to $\Delta L = 6\%$.

Both CRH and IH sintering data in Figs. 3 and 4 show about 3.8 to approximately 6 for the $n$ value. The $n=4$ value can be explained both by Bannister's models [25] and our model (Part I) [18] for sintering controlled by grain-boundary diffusion. Furthermore, a sintering equation based on the latter model

$$\Delta L^3 d(\Delta L) = \frac{\left(\frac{R}{R_j}\right)^3 \int_0^{\theta_i} \frac{d\theta}{r_p} + \int_{\theta_i}^{\pi/5} \frac{d\theta}{\rho}}{\int_0^{\pi/6} \frac{d\theta}{\rho}} \frac{K_d dT}{R^4} \tag{5}$$

or

$$\Delta L_j^{4+\varepsilon} - \Delta L_i^{4+\varepsilon} = K_d(t_j - t_i)/R^4 \tag{5'}$$

explains well the increase of the $n$ value with increasing the microregions of the intermediate-stage, where $\Delta L_i$ and $\Delta L_j$ are, respectively, shrinkages at time $t_i$ and $t_j$, $K_d$

is a constant, $r_p$ is the radius of the curvature of a pore surface, and superior $\varepsilon$ is an exponent correction at sintering time, $t_j$. Since $t_i$ equals zero for a green compact, the $\Delta L_i$ value for $t_i = 0$ means the effective shrinkage of the green compact with grown necks.

No exact $K_d$ value has been reported, and thus a suitable one was assumed on calculation of Eq. (5) for the grain-boundary diffusion mechanism. The solid lines in Fig. 4 show the calculated values, which exactly describe the present isothermal shrinkage curves in it, except at 1070°C.

The measured data listed in Fig. 7 indicate that $S_p$ decreased by 2.44% when the powder was pressed at 200 MPa. If the reduction in $S_p$ is caused by sintering, Fig. 6 indicates the $\Delta L_i$ value of 0.1% for 2.44% of $S_p$. The present theory, however, mathematically estimates 3 for the apparent exponent, $n'$, with conditions $\Delta L_j = 0.4\%$, $\Delta L_i = 0.1\%$ and $n = 4$. This value is smaller than the experimental $n'(=3.8)$ one. Artz [29] suggested a difference between the neck geometries caused by compaction ($\rho = 0$) and by sintering ($\rho \approx y$). Eq. (1) indicates that $\Delta\mu$ at $\rho \approx 0$ is much lower than that at $\rho \approx y$. The shrinkage rate is, therefore, faster for the case of $\rho \approx 0$ than that of $\rho \approx y$ even if contact areas, that is, the apparent $\Delta L_i$ values are equal in both the cases. An effective $\Delta L_i$ value for densification in the green compact thus was smaller than the apparent $\Delta L_i$ value (0.1%) estimated from the aforesaid reduction of $S_p$. $\Delta L_i < 0.1\%$ means $n' > 3.0$. The exact $\Delta L_i$ value for a given $S_p$ value cannot be estimated, because few data are available for neck geometry formed by pressure on a powder compact; but the experimental value of $n' = 3.8$ ($> 3$) qualitatively agrees with that the effective $\Delta L_i$ value was smaller than 0.1%. The term of $\Delta L_i$ in Eq. (5') was, therefore, practically negligible for the present sample and $\Delta L^n = K_d t/R^4$. From this equation, the time exponent, $1/n$, is estimated as

$$n = (dt/t)/(d\Delta L/\Delta L) \quad (6)$$

Eq. (6) defines the $n$ value as the reverse of a tangent of the solid lines in Fig. 4. Fig. 8 shows the calculated $n$ value varying with $\Delta L$. Increase in the $n$ value from 4 to 6 means rapid decrease of a shrinkage rate as compared with the constant case of $n = 4$. The high purity of the present $Al_2O_3$ powder suggests negligible segregation of impurities in grain boundary layers irrespective of the sintering stage. This means that the widths of diffusion fields were unchanged for enhanced diffusion of the atoms in the aforesaid layers during sintering. The transformation of neck geometries from the initial to the intermediate stage of sintering, on the other hand, results in a marked decrease of the driving force from $\gamma/\rho$ of the initial stage to $\gamma/r_p$ of the intermediate stage because of a large inequality, $\rho << r_p$. This marked decrease of the driving force was a major origin for the aforesaid rapid reduction of a densification rate.

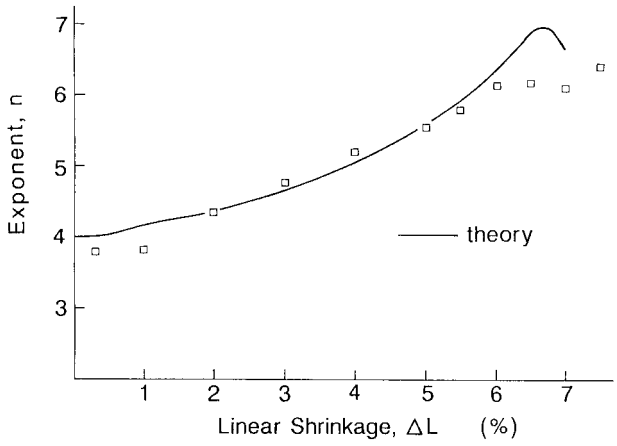


Fig. 8. Change of the $n$ value during progressing of sintering. Dots were experimentally obtained from the data of CRH sintering and the solid line was theoretically calculated from Eq. (5).

Fig. 8 also shows a decrease of the theoretical $n$ value from $\Delta L = 6.75\%$, that is, reducing deceleration of a shrinkage rate during sintering. This tendency is explained by the two characteristics of densification in the intermediate stage. One of them is that neck growth is slower in the intermediate stage than in the initial stage — distances between diffusion sources and diffusion sinks increase in proportion to neck growth. The other is that the curvatures of neck surfaces decrease in initial-stage sintering, and the driving forces quickly decrease with sintering. Whereas densification in the intermediate stage essentially decreases pore sizes, increasing the driving forces.

The plots in Fig. 8 were experimentally estimated with the CRH shrinkage data in Fig. 3, showing the apparent difference between the theoretical (solid) line and the experimental data for $\Delta L = 0.3$ and $= 1\%$. This difference well accords with the isothermal sintering data of Fig. 4, which deviated at 1070°C from the theoretically calculated values shown with the solid line. The solid line in Fig. 8, on the other hand, describes quantitatively the experimental $n$ value from $\Delta L = 2$ to 6%, despite the appearance of many necks with intermediate-stage geometries (see Fig. 5). The closely fitted values in this wide range of $\Delta L$ are attributed to that necks in the initial stage effectively governed the present sintering in such a wide range of $\Delta L$. This is because the driving force, $\gamma/\rho$, of the initial stage is markedly larger than that, $\gamma/r_p$, of the intermediate stage, and the actual driving force is proportional to the number of necks in the initial stages, that is, the $C_I$ value defined by Eq. (2).

If, on the other hand, the $C_I$ value becomes negligibly small, the distributions of grain sizes and pore sizes have relatively appreciable influence on the effective driving force for densification. Both Figs. 6 and 8 show the calculated values deviating from the experimental data above $\Delta L = 6\%$. These deviations suggest slight influence of necks in the initial stage on the actual densification,

which should be thereby described by a single sintering model for the intermediate stage.

As mentioned earlier, the appreciable reduction of the $S_p$ value occurred initially from 5.35 to 4.70 $M^2/g$ both by smoothing of rough surfaces and disappearance of peculiarly small particles, followed by contribution of neck growth to the reduction concerned. The latter data consist with the data in Fig. 6, in which the $S_p$ value reduced from 4.70 $M^2/g$ together with shrinkage of the powder compact. Part I [18] of the present study evaluated a specific surface area, $S_p$, as

$$S_p = M\left(1 - \frac{3\theta_i}{\pi}\right)k_c R^2 - \frac{3n_c M}{\pi}\int_{\theta_i}^{\pi/6} s_i \mathrm{d}\theta + \frac{3n_c M}{\pi}\int_0^{\theta_i}\left(\frac{R}{R_i}\right)^3 S_m \mathrm{d}\theta \quad (7)$$

where the $M$ value is the number of particles per unit weight for the powder compact, $k_c$ is the shape factor related to the total area (surface areas plus interfacial areas) characteristics to the particles, $s_i$ is a reducing area per a neck by neck growth in the initial stage of sintering. The first and the second terms in the right-hand side of Eq. (7) estimate the sum of the total areas of particles and the integration of areas, $s_i$, in the initial stage, respectively. The last term in it concerns the total of the pore surface areas, $S_m$, in the intermediate stage. $k_c R^2 M$ naturally equals the specific surface area of the powder. After rough surfaces become the flat ones, the $k_c$ value is a constant. The $S_m$ value was estimated in a previous paper [28] as

$$S_m = k_{s1} r_p - k_{s2} r_p R_i \quad (8)$$

where $k_{s1}$ and $k_{s2}$ are constants.

For the regular close packing of equal-size spheres; i.e. either hexagonal or face-enter-cubic packing, $\rho_s$ equals 0.74 of theoretical; the $n_c$ value for this packing equals 12. These $\rho_s$ and $n_c$ values are larger than those for random packing. Scott [16] reported $\rho_s = 0.63$ and $n_c = 9.3 \pm 0.8$ for random close packing. Our previous study [28] proposed bimodal array for the packing of the present particles; a simple cubic array, $n_c = 6$, for most of the particles; and a dodecahedral array, $n_c = 12$, for the balance. Since the $\rho_s (= 59.2\%)$ value of the present green compact was less than 0.63, $n_c$ was roughly estimated as 7. The value of $k_c$ was estimated as $12 (\approx 4\pi)$. The values of $k_{s1} (= 1.77)$, $k_{sv} (= 2.173)$ and $r_p$, on the other hand, were estimated according to our sintering model [28] for the intermediate stage. The solid line, a, in Fig. 6 shows the $S_p$ calculated from Eqs. (7) and (8) with these estimated values, closely fitting the measured $S_p$ values, especially in the range $\Delta L = 0$–$6\%$. Curve b in Fig. 6, on the other hand, was based on the pyramid-plate model of Bannister [25], assuming $n = 9$ and a dihedral angle of 150°. The convex curve of variation of b is in contrast to the concave one for the experimental data.

Similar calculations were also made for spherical particles, with a particle size distribution assumed equal to that reported previously [28]. Line c in Fig. 5 shows an abrupt change from the initial to the intermediate stage for this case, indicating fewer necks of the intermediate stage in the range from $\Delta L = 0\%$ to approximately 4.5% than line a of the present model. This difference results in slower grain growth of the spherical particles (line d, Fig. 5) than that of the polyhedral particles (line b, Fig. 5). The measured $R_m$ values, dots, in this figure were closer to line d than to line b. Variation of the $R_m$ value in this figure was only 5% of $R_m$ up to shrinkage of $\Delta L = 6\%$. Furthermore, an error of several per cent must be considered for measurement of an average particle size with SEM fractographs. The data of grain growth, then, produced poor information to evaluate which, sphere or polyhedron, is valid as the particle shapes of the present particles.

Line c in Fig. 6, on the other hand, shows $S_p$ for a sintered compact of the spherical particles with concave neck surface, as calculated with $n_c = 12$ and using the grain growth data (line d, Fig. 5). A rapid decrease in $S_p$ from $\Delta L = 3.5$ to 5% is attributed to an abrupt change in the neck geometry from the initial to the intermediate stage. Despite the large $n_c$ value, the calculated $S_p$ values are appreciably larger than the experimental values in the range $\Delta L = 0\%$ to approximately 4%. Fig. 6 furthermore shows that the $S_p$ values of variation c are smaller than those of variation d similarly calculated for spherical particles with convex neck surface [30]. If the dispersion of particle sizes is relatively narrow, $n > 12$ is hardly obtained, which suggests that the present particles cannot be replaced by spherical ones regardless of the curvature of neck surfaces. This conclusion is in accordance with the shrinkage data of $n = 4$ to approximately 6.

The distinct lines in Fig. 6 indicate that a sintering model is very sensitive to the relation between $S_p$ versus $\Delta L$; measuring this relationship thus can effectively describe a sintering model. Part I [18] of the present study, however, indicates that such measurement is ineffective for determining the predominant mechanism, which, on the other hand, can easily be accomplished using the relationship of $\Delta L$ versus time. The mechanism revealed, however, is misleading for $n = 3$, because two possibilities exist — i.e. the volume-diffusion mechanism for the present model [18] and Bannister's [25] and the grain-boundary diffusion mechanism for the usual models [4,5,26]. Measurement of both the relations, $\Delta L$ versus time and $S_p$ versus $\Delta L$, are thus necessary to produce a reasonable sintering model and to identify a predominant mechanism.

Naturally, shapes of particles were not unique even in the present powder. Furthermore, the edge of a particle

contacts the face of a neighboring particle at an as-yet undefined position, such as the center or side. Close fit between the theoretical and the experimental data, however, supports the fundamental validity of the present sintering model.

## 5. Conclusions

The sintering data of a highly sinterable $Al_2O_3$ powder were quantitatively described with the sintering model proposed in Part I, and the following conclusions were obtained.

1. Grain-boundary diffusion contributes predominantly to densification of the present powder.
2. When both the combination of the initial and intermediate stages and the grain-boundary diffusion mechanism are predominant, the inverse power dependence of time increases from 4–6 in the range $\Delta L = 2$–$6\%$.
3. Appreciable number of necks with very low $\theta$ values induces abrupt decrease in specific surface area until $\Delta L = 1.5\%$.

## References

[1] C. Greskovich, K.W. Lay, Grain growth in very porous $Al_2O_3$ compacts, J. Am. Ceram. Soc. 55 (3) (1972) 142–146.
[2] L.R. Furlong, L.P. Domingues, Sintering of yttrium oxide, Am. Ceram. Soc. Bull. 45 (12) (1966) 1051–1154.
[3] G.C. Kuczynski, Self-diffusion in sintering of metallic particles, J. Metals, 1 (2) Trans. AIME 185 (2) (1949) 169–178.
[4] W.D. Kingery, M. Berg, Study of the initial stages of sintering solids by viscous flow, evaporation-condensation, and self-diffusion, J. Appl. Phys. 26 (10) (1955) 1205–1212.
[5] R.L. Coble, Initial sintering of alumina and hematite, J. Am. Ceram. Soc. 41 (2) (1958) 55–62.
[6] H.E. Exner, G. Petzow, in: G.C. Kuczynski (Ed.), Material Science Research, vol. 13, Plenum Press, New York, 1980, pp. 107–120.
[7] J.M. Dynys, R.L. Coble, W.S. Coblenz, R.M., Cannon, in: G.C. Kuczynski (Ed.), Material Science Research, vol. 13, Plenum Press, New York, 1980, 391–404.
[8] S. Prochazka, R.L. Coble, Surface diffusion in the initial sintering of alumina, Part III, kinetic study, Physics of Sintering 2 (2) (1970) 15–34.
[9] R.M. German, Z.A. Munir, Surface area reduction during isothermal sintering, J. Am. Ceram. Soc. 59 (9–10) (1976) 379–383.
[10] F.F. Lange, Sinterability of agglomerated powders, J. Am. Ceram. Soc. 67 (2) (1984) 83–89.
[11] T. Ikegami, Y. Mori, S. Matsuda, H. Suzuki, Heats of wetting of various BeO powders in water, Yogyo-Kyokai-Shi, 81(11) 4 (1973) 55–58.
[12] W.H. Rhodes, Agglomerate and particle size effects on sintering yttria-stabilized zirconia, J. Am. Ceram. Soc. 64 (1) (1981) 19–22.
[13] E.A. Barringer, R. Brook, H.K. Bowen, The sintering of monodispersed $TiO_2$, in: G.C. Kuczynski, A.E. Miller, G.A. Stargent (Eds.), Sintering and Heterogeneous Catalysts, Plenum Press, New York, 1984, pp. 1–21.
[14] W. Rafaniello, M.S. Paquette, T.D. Rey, Examination of commercial AlN powders, in: G.L. Messing, S. Hirano, H. Hausner (Eds.), Ceramic Transactions, Vol. 12. Ceramic Powder Science III. Amer. Ceram. Soc. Inc., 1990, pp. 865–874.
[15] S. Horikiri, Production process and characteristics of high purity alumina, FC Annual Report 1986, 1986, pp. 23–31.
[16] G.D. Scott, Radial distribution of the random close packing of equal spheres, Nature 194 (9) (1962) 956–957.
[17] T. Ikegami, Y., Kitami, M. Tsutsumi, Early-stage sintering: II. Reduction in specific surface area of an alumina powder at a relatively low temperature, Ceramics International 25 (2) (1999) 183–190.
[18] T. Ikegami, Early-stage sintering in a powder compact of polyhedral particles: I. Models, Ceramics International 25 (5) (1999) 415–424.
[19] W.H. Gitzen, in: Alumina as a Ceramic Material, The American Ceramic Society Inc., Ohio, 1970, pp. 29–35.
[20] C. Herring, Surface tension as a motivation for sintering, in: T.E. Kingston (Ed.), The Physics of Powder Metallurgy, McGraw-Hill, New York, 1951 (Chapter 8).
[21] A.F. Moodie, C.E. Warble, MgO morphology and the thermal transformation of $Mg(OH)_2$, J. Crystal Growth 74 (1986) 89–100.
[22] S. Iijima, Ultra-fine spherical particles of $\gamma$-alumina: electron microscopy of crystal structure and surface morphology at atomic resolution, J. Appl. Phys. 23 (6) (1984) L347–350.
[23] G. Wulff, Zur Frage der Geschwindigkeit des Wachstums und der Aufloesung der Krystallflaechen (About the Velocity of Growth and Dissolution of Crystal Faces), Z. Kristallogr. 34 (1901) 449–530.
[24] D.L. Johnson, I.B. Cutler, Diffusion sintering: I. Initial stage sintering models and their application to shrinkage of powder compacts, J. Am. Ceram. Soc. 46 (11) (1963) 541–545 "II" ibid., 545–550.
[25] M.J. Bannister, Shape sensitivity of initial sintering equations, J. Am. Ceram. Soc. 51 (10) (1968) 548–553.
[26] M.F. Ashby, A first report on sintering diagram, Acta Metall. 22 (3) (1974) 275–289.
[27] R.M. German, Z.A. Munir, Identification of the initial stage sintering mechanism using aligned wires, J. Mater. Sci. 11 (1976) 71–77.
[28] T. Ikegami, Y. Moriyoshi, Intermediate-stage sintering of a homogenously packed compact, J. Am. Ceram. Soc. 67 (3) (1984) 174–178.
[29] E. Artz, The influence of an increasing particle coordinaton on the densification of spherical powders, Acta Metall. 30 (10) (1982) 1883–1890.
[30] B. Wong, J.A. Pask, Models for kinetics of solid state sintering, J. Am. Ceram. Soc. 62 (3–4) (1979) 138–141.